

RESEARCH ARTICLE

Laminin N-terminus $\alpha 31$ is upregulated in invasive ductal breast cancer and changes the mode of tumour invasion

Lee D. Troughton^{1,2*}, Danielle A. O'Loughlin², Tobias Zech³, Kevin J. Hamill²**1** Cell and Molecular Physiology, Loyola University Chicago, Chicago, Illinois, United States of America,**2** Institute of Life Course and Medical Sciences, University of Liverpool, Liverpool, United Kingdom,**3** Institute of Systems, Molecular and Integrative Biology, University of Liverpool, Liverpool, United Kingdom* ltroughton@loyola.luc.edu

Abstract

Laminin N-terminus $\alpha 31$ (LaNt $\alpha 31$) is an alternative splice isoform derived from the laminin $\alpha 3$ gene. The LaNt $\alpha 31$ protein is enriched around the terminal duct lobular units in normal breast tissue. In the skin and cornea the protein influences epithelial cell migration and tissue remodelling. However, LaNt $\alpha 31$ has never been investigated in a tumour environment. Here we analysed LaNt $\alpha 31$ in invasive ductal carcinoma and determined its contribution to breast carcinoma invasion. LaNt $\alpha 31$ expression and distribution were analysed by immunohistochemistry in human breast tissue biopsy sections and tissue microarrays covering 232 breast cancer samples. This analysis revealed LaNt $\alpha 31$ to be upregulated in 56% of invasive ductal carcinoma specimens compared with matched normal tissue, and further increased in nodal metastasis compared with the tumour mass in 45% of samples. 65.8% of triple negative cases displayed medium to high LaNt $\alpha 31$ expression. To study LaNt $\alpha 31$ function, an adenoviral system was used to induce expression in MCF-7 and MDA-MB-231 cells. 2D cell migration and invasion into collagen hydrogels were not significantly different between LaNt $\alpha 31$ overexpressing cells and control treated cells. However, LaNt $\alpha 31$ overexpression reduced the proliferation rate of MCF-7 and MDA-MB-231 cells. Moreover, LaNt $\alpha 31$ overexpressing MDA-MB-231 cells displayed a striking change in their mode of invasion into laminin-containing Matrigel; changing from multicellular streaming to individual cellular invasion. In agreement with these results, 66.7% of the tumours with the highest LaNt $\alpha 31$ expression were non-cohesive. Together these findings indicate that breast cancer-associated changes in LaNt $\alpha 31$ expression could contribute to the processes involved in tumour invasion and may represent a new therapeutic target.

OPEN ACCESS

Citation: Troughton LD, O'Loughlin DA, Zech T, Hamill KJ (2022) Laminin N-terminus $\alpha 31$ is upregulated in invasive ductal breast cancer and changes the mode of tumour invasion. PLoS ONE 17(3): e0264430. <https://doi.org/10.1371/journal.pone.0264430>

Editor: Rajeev Samant, University of Alabama at Birmingham, UNITED STATES

Received: March 29, 2021

Accepted: February 10, 2022

Published: March 1, 2022

Copyright: © 2022 Troughton et al. This is an open access article distributed under the terms of the [Creative Commons Attribution License](https://creativecommons.org/licenses/by/4.0/), which permits unrestricted use, distribution, and reproduction in any medium, provided the original author and source are credited.

Data Availability Statement: All relevant data are within the manuscript and its [Supporting information](#) file.

Funding: This work was supported by Biotechnology and Biological Sciences Research Council Grants BB/L020513/1 and BB/P0257731, and by North West Cancer Research, all grants awarded to KJH. These funding sources supported the purchase of consumables and equipment access and paid salaries of LDT. The funders played no role in the study design, data collection

Introduction

An essential stage of tumour progression is acquisition of an ability to breakthrough an organised extracellular matrix (ECM) structure termed the basement membrane (BM) [1]. Determining the expression and distribution of BM proteins has yielded valuable biomarkers to

and analysis, decision to publish, or preparation of the manuscript. <https://bbsrc.ukri.org/> https://www.nwcr.org/?gclid=Cj0KCQjw9YWWDBhDyARIsADt6sGZhiHHYwcv86EXoJE6fNO1f2Ju1jRgMgpOJ7TmFJFfe3lxc-YqBV4aAm15EALw_wcB.

Competing interests: The authors have declared that no competing interests exist.

Abbreviations: BM, Basement membrane; ECM, Extracellular matrix; EGF, Epidermal growth factor; eGFP, Enhanced green fluorescent protein; EGFR, Epidermal growth factor receptor; ER, Estrogen receptor; FFPE, Paraffin-fixed formalin-embedded; Her2, Human epidermal growth factor receptor 2; Ki67, Antigen ki-67; LaNt α 31, Laminin N terminal protein α 31; LE-repeat, Laminin-type epidermal growth factor-like; LM, Laminin; LN domain, Laminin N-terminal; p53, Tumour protein p53; PR, Progesterone receptor; RT-qPCR, Reverse Transcription-quantitative polymerase chain reaction; TDLU, Terminal duct lobular unit; TNBC, Triple negative breast cancer.

predict breast cancer outcomes [2–6]. Much of this work has focused on the laminin (LM) family of BM proteins, which are not only essential barrier components, but also act as substrates for tumour cell migration, regulate actin dynamics, influence survival and growth signalling pathways, and maintain quiescence in cancer stem cell niches; all of which influence breast cancer progression [7–10]. Here we investigated a relatively unstudied LM-related protein, laminin N-terminus α 31 (LaNt α 31) that we predicted would change in cancer and which could therefore represent a new target for therapeutic development [11, 12].

LMs are obligate heterotrimeric proteins comprised of an α , β and γ chain, with each chain derived from one of five α genes (LAMA1–5), one of three β (LAMB1–3), and one of three γ (LAMC1–3), as reviewed in [7, 8, 13]. Through the use of distinct promoters, LAMA3 generates two structurally distinct LMs; a so-called “full-length” variant LM α 3b, and the much shorter LM α 3a [8, 13–15]. The LaNt proteins are also derived from LM-encoding genes, through intron-retention and polyadenylation within the retained intron [11]. Four LaNt family members have been identified at the transcript level; however, only LaNt α 31, derived from the LAMA3 gene, has been confirmed at the protein level [11]. LaNt α 31 displays widespread tissue distribution and is enriched in structured regions of ECM surrounding terminal duct lobular units (TDLUs) in normal breast tissue [11].

LaNt α 31 functions have only been studied in corneal and skin epithelium to date, where upregulation of LaNt α 31 was observed in response to corneal burn wounds or stem cells activation in ex vivo models, and where knockdown in expression reduced the rate at which epidermal keratinocytes close scratch wounds [11, 12]. Mechanistic studies have also indicated a role for this protein in modifying cell adhesion and migration via changes to matrix organisation and adhesion complex maturation [12, 16]. Further indications to LaNt α 31 function come from its structure. Although LaNt α 31 is smaller than LMs and lacks the coiled-coil domain required for LM trimer formation, it does share structural domains with LM α 3b. Specifically, LaNt α 31 is comprised of a LM N-terminal domain (LN domain) and two LM-type epidermal growth factor-like repeats (LE domains) [11]. LN domains are involved in LM-to-LM interaction, and therefore are essential for laminin network assembly in BMs [7, 17, 18]. LaNt α 31 also contains 54 unique amino acids with no homology to known structural motifs but which have allowed specific antibodies to be raised against this protein [11, 12]. Intriguingly the LaNt α 31 protein architecture is structurally similar to other members of the laminin superfamily family, the netrins. Netrins are predominantly known as signalling proteins; however, netrin-4, via its LN domain, can disrupt LM-LM interactions and change the structural characteristics of LM networks [19–21]. Moreover, netrin-4-induced changes to BM stiffness is a strong predictor of tumour metastasis and patient outcome in numerous cancers including breast cancer [22].

While functional data suggest that LaNt α 31 could be capable of influencing tumour progression, further rationale for investigating this protein in tumour microenvironment comes from studies of the other, more comprehensively studied, products of the LAMA3 gene. Reduction of LM α 3a and LM α 3b in breast carcinoma has been independently reported by several groups [23–25], with LM α 3b downregulation in tumour vasculature associated with later stage tumours [26]. However, the situation is more complicated than a simple linear relationship, as increased LM α 3 has been associated with triple negative breast carcinoma, and increased immunoreactivity that correlated with tumour stage has also been reported with antibodies against conformational epitopes in LM α 3 β 3 γ 2 (LM332), LM β 3 and LM γ 2, the preferred trimerisation partners of LM α 3a and LM α 3b [25, 27].

Here we performed the first investigation into LaNt α 31 in breast cancer. Breast tissue from normal and invasive ductal carcinomas were processed for immunohistochemistry with antibodies against LaNt α 31, and correlations between staining intensity and pathology

determined. LaNt α 31 expression was upregulated in cultured breast carcinoma cells and the impact on cellular behaviour was determined. The results revealed that LaNt α 31 is increased in tumour tissue, and is further increased in metastasis. Moreover, whereas induced LaNt α 31 expression did not drive non-invasive breast cancer cells to become invasive, it did influence invasive breast cancer cells to change the mode of their invasion into LM-rich matrices. These findings indicate that this little studied protein plays a role in defining how breast cancers disseminate.

Methods

Ethical approval

The Liverpool Bio-Innovation Hub Biobank conferred ethical approval in writing for the use of samples in this project (REC reference 14/NW/1212, NRES Committee North West–Haydock). Project specific ethical approval for working with human tissue was conferred in writing by the University of Liverpool Research Ethics Committees (approval number:7488). All archived patient tissues were collected with informed consent. Data were fully anonymised before granting access.

Antibodies

Mouse monoclonal antibodies raised against human LaNt α 31 were described previously and were used at $0.225 \mu\text{g mL}^{-1}$ for IHC [12, 28]. Mouse monoclonal antibodies against human LM α 3 (clone CL3112) and mouse IgG (both Sigma-Aldrich, St. Louis, Missouri, USA) were used at $0.5 \mu\text{g mL}^{-1}$. Mouse monoclonal antibodies against GFP were used at $0.2 \mu\text{g mL}^{-1}$ for immunoblotting (clones 7.1 and 13.1, Sigma-Aldrich).

Immunohistochemistry

Pilot tissues were obtained from the Liverpool Bio-Innovation Hub Biobank, all other TMA sections were purchased from Reveal Bioscience (product codes: BC02, BC03, BC05, BC06, and BC10; Reveal Bioscience, San Diego, USA) or US Biomax (product code: HBreD145Su02; US Biomax, Rockville, Maryland, USA). Sections were dewaxed and processed using a Leica Bond autostainer with Bond™ Polymer Refine Detection system (Leica Biosystems, Wetzlar, Germany). Briefly, following dewaxing, antigen retrieval was performed by incubating with a Tris/EDTA (pH 9 solution) solution for 20 min at 60°C , then endogenous peroxidases were blocked for 5 min at room temperature with Bond hydrogen peroxide solution. Sections were incubated with primary or isotype-matched control antibodies at room temperature for 30 min in Bond primary Ab solution (Tris-buffered saline, TBS, containing surfactant and protein stabiliser), then secondary anti-mouse IgG antibodies ($<10 \mu\text{g mL}^{-1}$) with 10% v/v animal serum in TBS were added for 15 min at room temperature. DAB (66 mM) chromogen substrate was added for 20 min at room temperature, and counterstaining performed with 0.1% w/v haematoxylin for 5 min. At each stage, washing was performed with Bond wash solution (TBS containing surfactant). Sections were finally dehydrated through a series of ascending ethanol concentrations and then mounted with Pertex (all reagents Leica Biosystems). Stained tissue sections were imaged on the Aperio ImageScope slide scanner and processed using ImageScope software (Leica Biosystems).

Immunohistochemistry interpretation

TMA cores were graded from 0–3 based on LaNt α 31 immunoreactivity. Scores of 0 and 1 were then combined, and expression defined as low, medium, or high. All cores were scored

by three independent scorers, and the mean score from duplicate cores used in final analyses. All patient data, including tumour/ node/ metastasis (TNM) status, tumour grade, and IHC marker scores (antigen ki-67 [Ki67], epidermal growth factor receptor [EGFR], human epidermal growth factor receptor 2 [Her2], oestrogen receptor [ER], and progesterone receptor [PR]) were provided by Reveal Biosciences. Data were rounded to the nearest integer for intensity scores where required. For Ki67 percentage cell staining, scores were grouped as 0, 6–10, or >10%, as provided by Reveal Biosciences.

Cell culture

MCF-7 [29] and MDA-MB-231 [30] cells were cultured in high glucose (4.5 g L^{-1}) Dulbecco's Modified Eagle Medium (DMEM) (Sigma-Aldrich) supplemented with 10% Foetal Calf Serum (FCS, LabTech International Ltd, Heathfield, East Sussex, UK) and 4 mM L-glutamine (Sigma-Aldrich).

LaNt α 31 expression

Full length *LAMA3LN1-eGFP* and *eGFP* adenoviral particles were prepared and used as previously described [12]. Transduction efficiency was determined by live fluorescent imaging at the time of analysis and expression confirmed by immunoblotting after 24 h. Cells were homogenised by scraping into urea/ sodium dodecyl sulphate (SDS) buffer (10 mM Tris-HCl pH 6.8, 6.7 M Urea, 1% w/v SDS, 10% v/v Glycerol and $7.4 \mu\text{M}$ bromophenol blue, containing $50 \mu\text{M}$ phenylmethanesulfonyl fluoride and $50 \mu\text{M}$ N-methylmaleimide, all Sigma-Aldrich). Lysates were sonicated and 10% v/v β -mercaptoethanol added (Sigma-Aldrich). Proteins were separated by SDS-polyacrylamide gel electrophoresis (SDS-PAGE) using 10% polyacrylamide gels (1.5 M Tris, 0.4% w/v SDS, 10% acrylamide/ bis-acrylamide; electrophoresis buffer; 25 mM Tris, 190 mM glycine, 0.1% w/v SDS, pH 8.5 all Sigma-Aldrich). Proteins were transferred to nitrocellulose membranes (Biorad, California, USA) using the Biorad TurboBlot™ system and blocked for one hour at room temperature in Odyssey[®] TBS-Blocking Buffer (Li-Cor BioSciences, Lincoln, Nebraska, USA). The blocked membranes were incubated overnight at 4°C with primary antibodies diluted in blocking buffer, then probed for 1 hour at room temperature with IRDye[®] conjugated secondary antibodies against mouse IgG (800CW) raised in goat (LiCor BioSciences) diluted in Odyssey[®] TBS-Blocking Buffer buffer at $0.05 \mu\text{g mL}^{-1}$. Membranes were imaged using the Odyssey[®] CLX 9120 infrared imaging system and Image Studio Light v.5.2 (LiCor BioSciences) used to process scanned membranes.

Proliferation assays

Proliferation assay: Cells were transduced with *LAMA3LN1-eGFP* or *eGFP* adenoviral particles. After 24 h, transduced or non-transduced cells were plated in triplicate at 2×10^3 cells/well of a 96-well plate (Thermo Fisher Scientific, Waltham, Massachusetts, USA), with one group of non-transduced cells cultured in media containing Nocodazole at 20 ng mL^{-1} in culture media (Thermo Fisher Scientific). After 24 h Hoechst 33342 (Thermo Fisher Scientific) was added to the culture media, and cell nuclei imaged after ~ 20 min using the Cytivia IN Cell Analyzer 2500HS (BMG LABTECH, Marlborough, Massachusetts, USA). Representative proteins extracts were taken at the +24-hour timepoint. Cell nuclei were counted from 3 fields of view per well, for 3 separate wells per independent experimental repeat.

Proliferation inhibition assay: 1.25×10^5 cells/well of non-transduced cells were seeded per well of a 6-well plate and treated with mitomycin c at $10 \mu\text{g mL}^{-1}$ for either 2 h or overnight. After 24 h, total RNA was extracted (Monarch[®] Total RNA Miniprep Kit, NEB) and one-step RT-qPCR performed to assess LAMA3LN1 transcript abundance (Luna[®] Universal qPCR

Master Mix, NEB), using a Roche LightCycler[®] 96 (Basel, Switzerland). GAPDH and RPLP0 were used as reference transcripts. All primer pairs were previously validated for efficiency and specificity [12], sequences as follows: LAMA3LN1: F-CTGGTGGAGGGGTCTGCATT, R-GGCAGTACACACAGGCTAAGAT; GAPDH: F-CGAGCCACATCGCTCAGACACC, R-GGTCAATGAAGGGGTCAATTGATGGCAAC; RPLP0: F-GCAGCATCTACAACCCTGAAGTGCTTGA, R-GGTAGCCAATCTGCAGACAGACACTGG. The Δ Ct method [31] was used to normalise the data to GAPDH and RPLP0, and the mean then compared to the untreated RNA ($2^{\Delta\Delta Ct}$).

2D migration assays

For gap closure assays, cells were seeded into ibidi[®] 2-well culture inserts (ibidi, Martinsried, Germany); at 7.0×10^4 cells/well (MCF-7) or 8.0×10^4 cells/well (MDA-MB-231). Culture inserts were carefully removed after 6 h, cell debris washed away, and the gap margin imaged using brightfield optics on a Nikon TiE epifluorescence microscope with a 10X objective at 0 and 16 h (Nikon, Tokyo, Japan). Gap closure was measured as a percentage relative to starting area using the freehand tool in image J (NIH, Bethesda, MA).

For low-density migration assays, cells were seeded at 5.0×10^4 cells/well of a 12-well plate, then imaged every 2 minutes over a 2-hour period using a 20X objective on a Nikon Eclipse Ti-E fluorescent microscope adapted for live cell imaging. Individual cells were tracked using the MTrackJ plugin on image J and migration speed calculated.

Inverted invasion assay

Inverted invasion assays were performed as previously described [32–34]. Briefly, 100 μ L of 1 mg mL⁻¹ rat tail collagen I (Corning Inc., New York, USA) or 4 mg mL⁻¹ Matrigel[®] from Engelbreth-Holm-Swarm (EHS) mouse sarcoma [35], was pipetted on top of Transwell[®] 24-well, 0.8 μ m, polycarbonate inserts (Corning). Then collagen was gelled through addition of 9.2 mM NaOH. Once gelled, the inserts were inverted and 100 μ L of cell suspension containing 8.0×10^5 cells were added to the lower surface. The transwells were then incubated for 4 h to allow the cells to attach before returning to the original position with basal side downward. 1 mL of serum-free media was pipetted into the lower chamber of the transwell, and 100 μ L of normal culture media supplemented with 25 ng mL⁻¹ EGF, as a chemoattractant, was added to the upper chamber [36]. After 72 h, the cells were fixed with 3.7% v/v formaldehyde for 30 min, permeabilised with 0.05% v/v Triton X-100 then stained for 1 hour with DAPI (Sigma-Aldrich). The inserts were mounted onto a glass coverslip and imaged with a Zeiss Marianas (3i) spinning-disk confocal microscope by taking a z-stack with images every 5 μ m, using SlideBook 5.5 software (3i, Intelligent Imaging Innovations Ltd, London, UK).

An algorithm was generated to automatically measure the DAPI stained nuclei in each slice of the z-stack. The average nuclei size was established by taking a range of manual measurements through the different planes of the z-stack. The average was used to set: i) the intensity threshold for distinguishing nuclei fluorescence from background as $t = 1000$, ii) the expected nuclei size $s = 240$ pixels, corresponding to an area of 101.4 μ m or a radius of 5.68 μ m, iii) the lower size threshold $s^- = 120$ pixels (area = 50.7 μ m or a radius of 4.02 μ m), below which captured objects were not considered to be nuclei and iv) the upper size threshold $s^+ = 400$ pixels (area 169 μ m or radius of 7.33 μ m), above which the captured object was assumed to be an artefact. For each image slice, the image was imported and a coarse segmentation of the nuclei performed by thresholding at the intensity value t to achieve a binary nuclei/non-nuclei image. Any nuclei within an absolute distance of 0.65 μ m or 1 pixel were connected to take

into account noise, and an initial index taken of the distinct identified nuclei candidates, while measuring the size of each nuclei.

Individual cells were then identified as follows: i) any identified object under s^- , $s/2$ pixels or over s^+ pixels in size was considered to be noise, ii) any captured object within the thresholds $s/2$ and $3s/2$ was considered to be one nuclei, iii) any remaining captured object which was larger than $3s/2$ in size was considered to be a cluster of nuclei which could not be split due to the resolution of the image. In these cases, the number of cells in the cluster was calculated as $(cluster\ size) / s$, rounded to the nearest integer. The following measures were then taken: i) total luminance of the cell image, ii) PixCount: the number of pixels considered to be a cell after thresholding, corresponding to the total area in microns of the region considered to contain a cell. iii) Cell Count: the total number of cells identified, including those estimated from cell clusters, iv) Entropy: a measure of randomness of the thresholding data, which identified how clustered the cells in the image were.

Data analyses

Microsoft Excel (Microsoft, Washington, USA), Graphpad Prism v.6 (Graphpad Software, California, USA), SPSS statistic 24 (IBM Corporation, New York, USA), or Jupyter Notebook (python) were used to analyse numerical data and generate graphs. Figures were generated using CoralDraw 2017 or Adobe Illustrator. The Wilcoxon signed-rank test or Somers' D was used for ordinal data, or Mantel-Cox log-rank test for survival data in immunohistochemistry analyses, and one-way rANOVA or ANOVA with Bonferroni post hoc test were used for continuous variables in gap closure, single cell migration, cell invasion depth, and proliferation data, or 2-way ANOVA with Tukey's post hoc test for entropy. Differences were deemed statistically significant where type I error rates were below 5%.

Results

LaNt α 31 and LM α 3 display distinct distribution patterns in invasive ductal carcinomas

First we compared the distribution of LaNt α 31 and LM α 3 in a pilot panel of four normal (Fig 1A), four invasive ductal carcinoma (Fig 1B) and four invasive ductal carcinoma that were triple negative for ER, PR, and Her2 (Fig 1C). The LM α 3 antibodies used recognise both the LM α 3a and LM α 3b forms. LaNt α 31 and LM α 3 displayed very similar distribution in the normal tissue (Fig 1A), primarily restricted to TDLU as previously reported [28], with the most intense immunoreactivity being present in the extracellular matrix surrounding the TDLU. However, much stronger and more widespread cellular LaNt α 31 expression was detected in three of the four invasive ductal carcinoma and three of the four triple negative specimens. In the invasive ductal tissue, LaNt α 31 displayed a more widespread distribution than LM α 3 (arrowheads, Fig 1B), whereas in ER-PR-Her2- cases the LM α 3 and LaNt α 31 distribution were very similar (Fig 1C). LM α 3 has been extensively investigated in breast cancer [23–25]; however, these new data for LaNt α 31 indicated potential additional value of investigating this isoform independently from LM α 3 in invasive ductal carcinoma.

LaNt α 31 expression is elevated in invasive ductal carcinoma and in nodal metastases compared to primary tumour tissue

To formally determine whether LaNt α 31 expression levels change in invasive ductal carcinoma, the relative intensity of cellular immunoreactivity in epithelial-like tissue was compared between normal breast tissue and tumour biopsies from the same person, with intensity scored

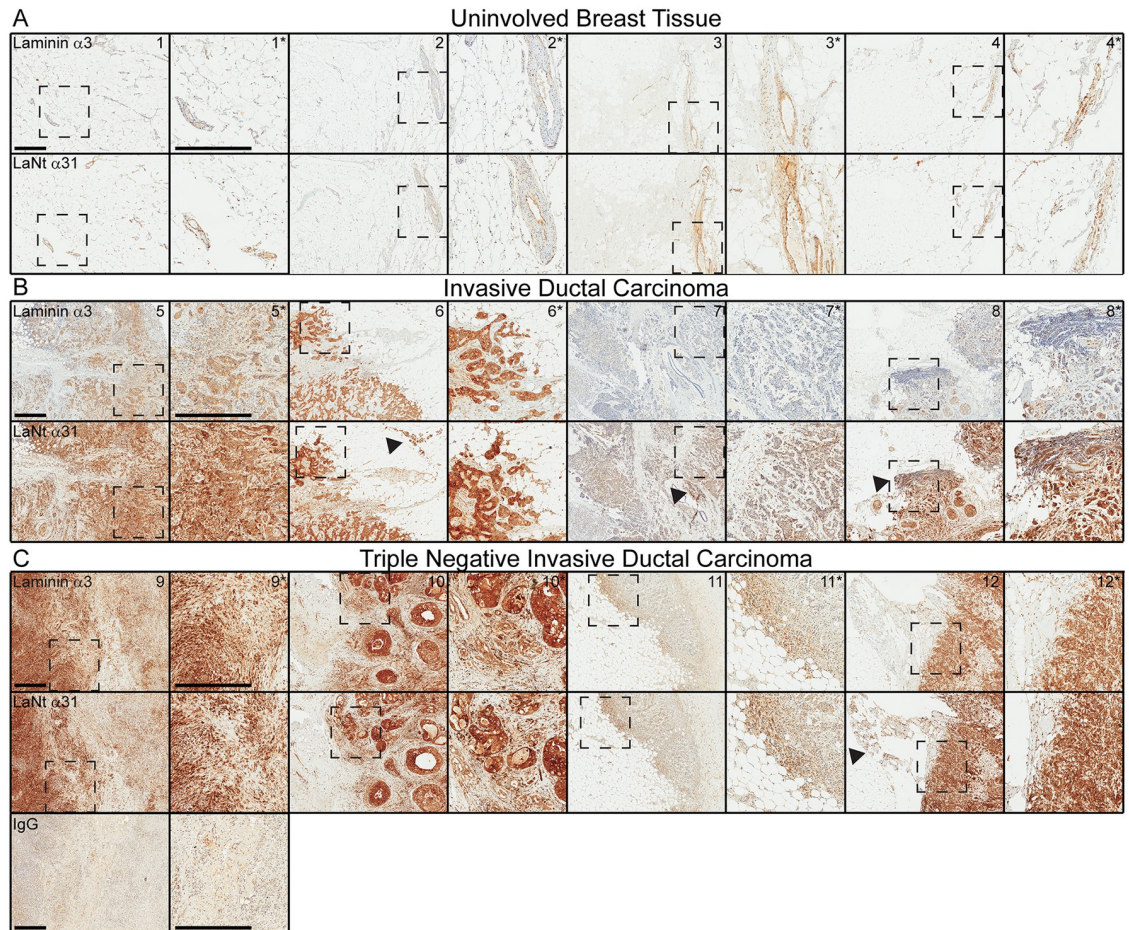


Fig 1. LaNt α 31 is upregulated in invasive ductal carcinoma. Serial sections from formalin-fixed paraffin-embedded human breast tissue processed for immunohistochemistry with mouse monoclonal antibodies against laminin α 3, LaNt α 31, or mouse IgG- isotype control, (A) uninvolved breast tissue, (B) invasive ductal carcinoma, and (C) ER-, PR-, Her- invasive ductal carcinoma. Dashed boxed regions are shown at higher magnification in columns to the right. Arrowheads indicate regions of anti-LaNt α 31 immunoreactivity not recognised by anti-laminin α 3. Scale bars: 500 μ m.

<https://doi.org/10.1371/journal.pone.0264430.g001>

by three independent, blinded scorers (representative examples, Fig 2A, all cores S1A Fig, patient ages Table 1). These paired analyses revealed LaNt α 31 expression to be increased in the cancer specimen in 14 of 25 tumours (56%), eight had no change, while three displayed decreased expression in the cancer tissue (Wilcoxon signed ranks test, $z = -2.67$, $p = 0.008$, Fig 2A).

Comparison of staining intensity between cores taken from the primary tumour against those from nodal metastasis from the same person using the same scoring approach, revealed that 13 of the 29 (45%) of the nodal metastasis displayed stronger LaNt α 31 staining compared with primary tumour tissue, 12 were scored the same, and four were decreased in the nodal tissue ($z = -2.18$, $p = 0.029$, Fig 2B, S1B Fig, patient ages Table 1).

High LaNt α 31 expression is associated with more proliferative tumours

To determine if LaNt α 31 immunoreactivity held prognostic value for invasive ductal carcinoma, we processed cores from 324 patients (Table 1, two cores per patient) and scored them

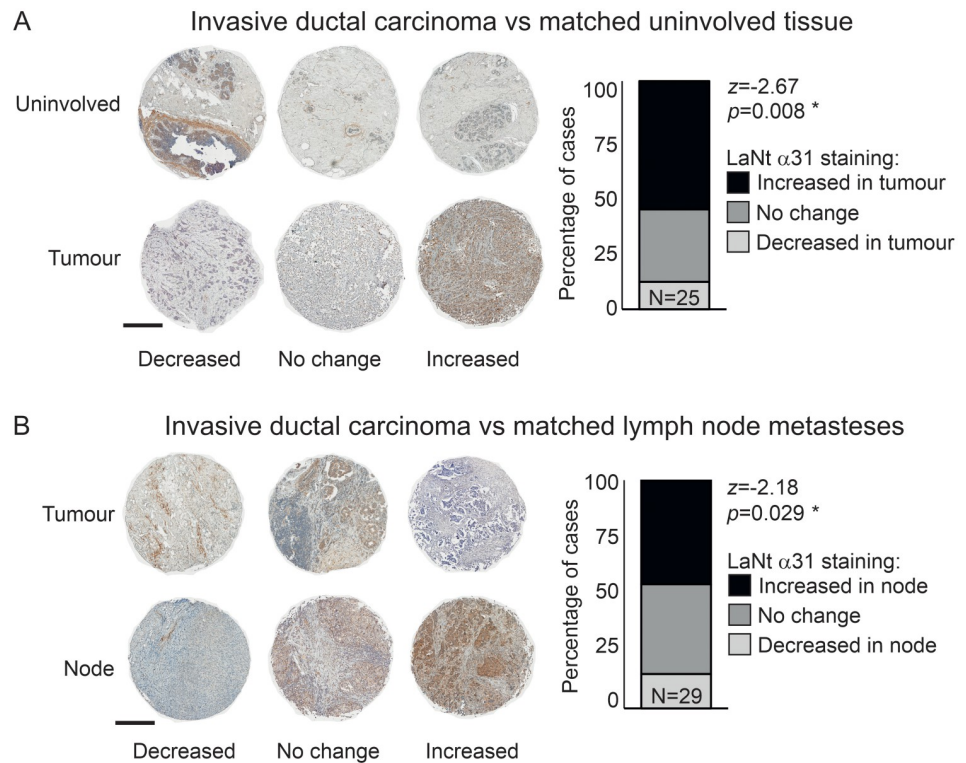


Fig 2. LaNt α 31 is upregulated in ductal carcinoma and in lymph node metastases. Formalin-fixed paraffin-embedded human breast tissue microarray sections processed for immunohistochemistry with mouse monoclonal antibodies against LaNt α 31. Two separate arrays were used; (A) uninvolved with paired invasive/ in situ ductal carcinoma tissues (N = 25), (B) invasive ductal carcinoma with paired node metastases (N = 29). Cores were scored as either decreased, no change, or increased staining intensity relative to the paired uninvolved (A) or primary tumour (B) core from the same donor (representative images shown). Stacked columns of percentage of cases in each category were plotted and Wilcoxon signed ranks test used to describe observed relationship. Scale bars: 500 μ m.

<https://doi.org/10.1371/journal.pone.0264430.g002>

by three independent scorers as “low”, “medium” or “high” LaNt α 31 intensity (representative images Fig 3A). First, we asked if LaNt α 31 staining intensity was predictive for tumour grade, Ki67 expression (as a marker of proliferation [37, 38]), nodal involvement, or survival (Fig 3B–3E). No association was observed between LaNt α 31 staining intensity and tumour grade (Somers’ d = 0.063, p = 0.44, Fig 3B); however, there was a positive correlation between Ki67

Table 1. Patient ages for each study cohort.

Study cohort	Mean	Median	Range	N
Invasive ductal carcinoma vs uninvolved ¹	46	45	29–70	25
Invasive ductal carcinoma vs lymph node metastases ²	47	46	30–69	29
Invasive ductal carcinoma grade, nodal involvement, biomarker correlative analyses ³	47	44	27–86	198*
Invasive ductal carcinoma survival analyses ⁴	60	57	33–88	126

¹Fig 1,

²Fig 2,

³Figs 3 and 4,

⁴Fig 3E.

*full data not available for all specimens

<https://doi.org/10.1371/journal.pone.0264430.t001>

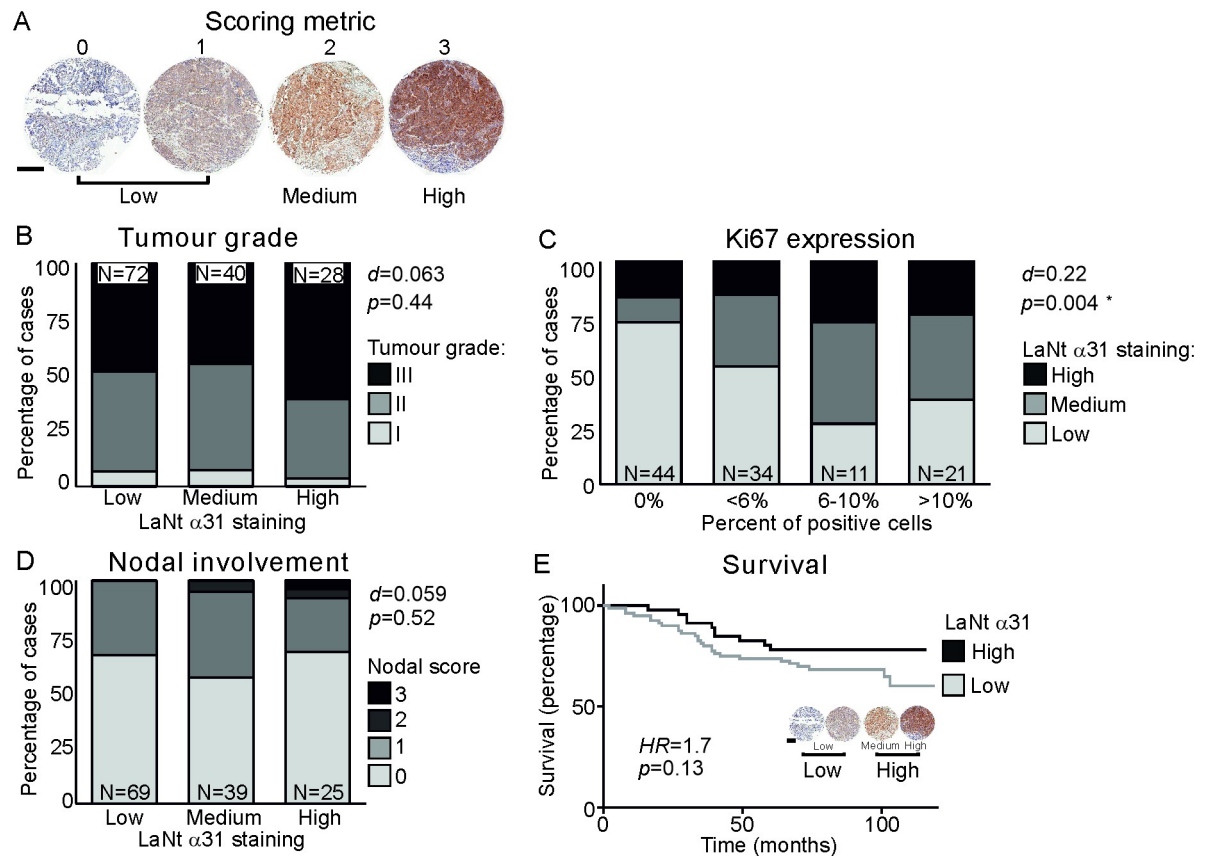


Fig 3. LaNt α 31 upregulation in invasive ductal carcinoma does not correlate with nodal involvement or tumour grade. Formalin-fixed paraffin embedded human breast tissue microarray sections processed for immunohistochemistry with mouse monoclonal antibodies against LaNt α 31. Cores were scored based on LaNt α 31 staining intensity from 0–3. Scores of 0 or 1 were combined and designated as low LaNt α 31 expression, score 2 as medium expression, and 3 as high expression. (A) Representative example of core scoring. (B–D) Stacked column graphs of percentage of cases with each staining intensity segregated by tumour grade I, II, or III (B), Ki67 expression (C), or by nodal involvement (D). Somers' D was used to describe observed relationships between LaNt α 31 staining intensity and the independent variables. (E) Kaplan–Meier survival curve, where LaNt α 31 staining intensity was simplified to low or high by pooling medium and high cores. Logrank test was used to determine hazard ratio and chi square for significance. Scale bar in (A): 300 μ m.

<https://doi.org/10.1371/journal.pone.0264430.g003>

expression level and LaNt α 31 intensity ($d = 0.22$, $p = 0.004$ Fig 3C). The relative proportion of high, medium and low LaNt α 31 did not correlate with nodal involvement ($d = 0.059$, $p = 0.52$, Fig 3D). Stratifying the cohort based on Ki67 expression levels before analysing association with nodal involvement, did not change this lack of association.

Survival was assessed for 126 cases where these data were available. To account for the smaller sample size, LaNt α 31 staining intensity was simplified to either low or high expression by combining the medium with the high expression cases. There were no statistically significant differences in survival between high and low expression groups (low = 66% survival, high = 78% survival, hazard ratio 1.75, confidence interval 0.9–3.4, $p = 0.13$, Fig 3E).

Next, we asked if LaNt α 31 staining displayed a relationship with any of the commonly used breast cancer biomarkers (Fig 4). These data revealed a weak but statistically significant positive association between LaNt α 31 and EGFR, and a weak but statistically significant negative association between ER and PR (EGFR $d = 0.17$, $p = 0.048$, ER $d = -0.23$, $p = 0.001$; PR $d = -0.15$, $p = 0.042$, Fig 4A) but no association with Her2 (Her2 $d = 0.086$, $p = 0.21$, Fig 4B).

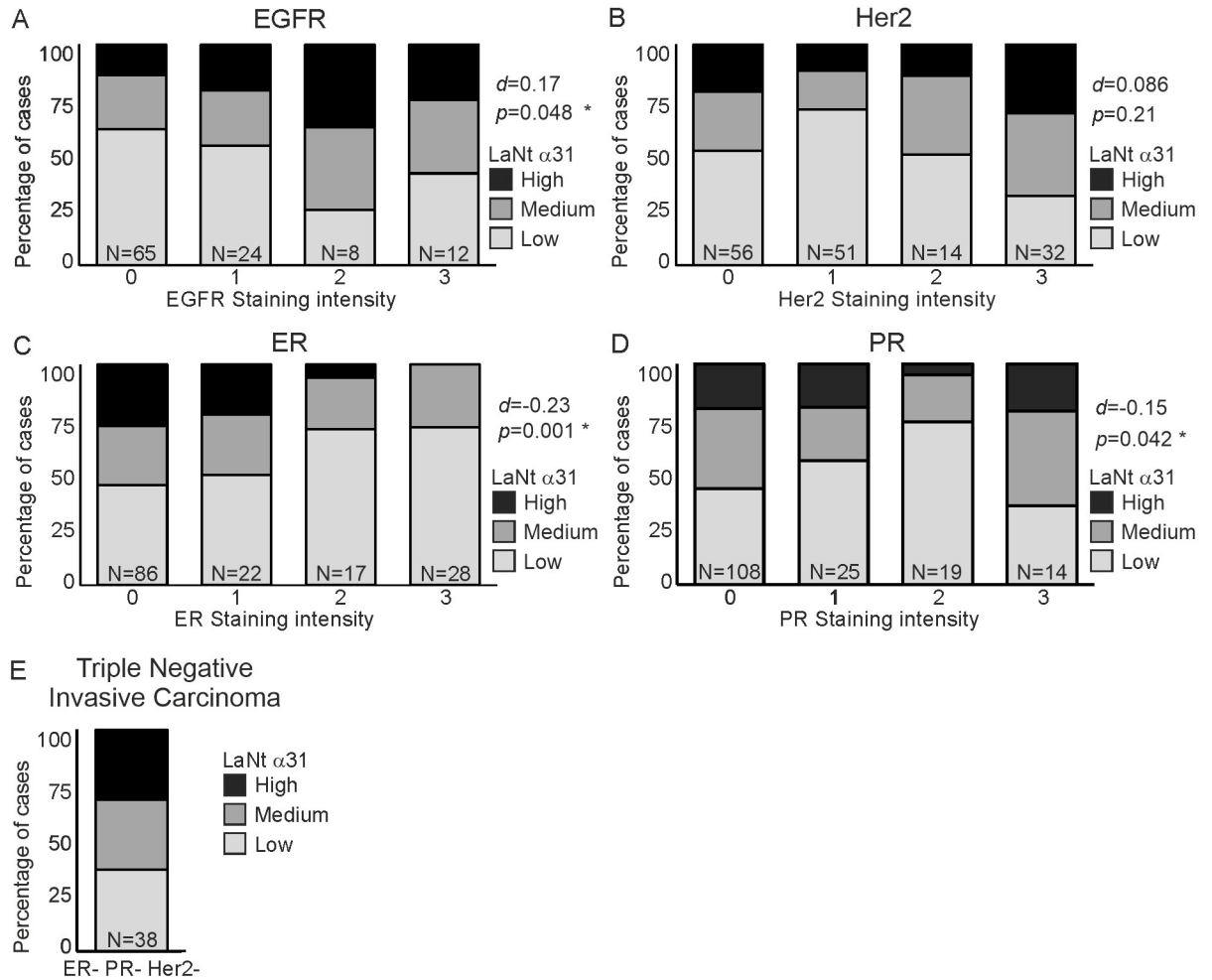


Fig 4. Positive correlation between LaNt α 31 staining intensity and EGFR expression. Formalin-fixed paraffin embedded human breast tissue microarray sections processed for immunohistochemistry with mouse monoclonal antibodies against LaNt α 31. Cores were scored based on LaNt α 31 staining intensity from 0–3. Scores of 0 or 1 were combined and designated as low LaNt α 31 expression (light grey bars), scores 2 as medium expression (dark grey bars), and 3 as high expression (black bars). Stacked column graph of percentage of cases that fall into group after segregation based on pathologist provided grading of immunohistochemistry markers; (A) EGFR, (B) Her2, (C) ER, (D) PR, or (E) ER- PR- Her2- cases. Somers' D was used to describe observed relationship between LaNt α 31 staining intensity and independent variable.

<https://doi.org/10.1371/journal.pone.0264430.g004>

The cores from triple negative cancers were analysed separately. These data revealed that 63% of the ER- PR- Her2- cores had either medium or high LaNt α 31 staining intensity (Fig 4E, n = 38 cores).

Induced LaNt α 31 expression reduces breast cancer cell proliferation

Although the immunohistochemistry findings indicated association between higher LaNt α 31 staining and higher Ki67 expression, this does not necessarily imply a causative relationship nor does it indicate directionality.

To investigate if LaNt α 31 expression is linked to proliferation, we used inhibited cell division using mitomycin c in two widely used cell lines derived from malignant ductal carcinomas, MCF7 and MDA-MB-231, then quantified *LAMA3LN1* transcript abundance using RT-

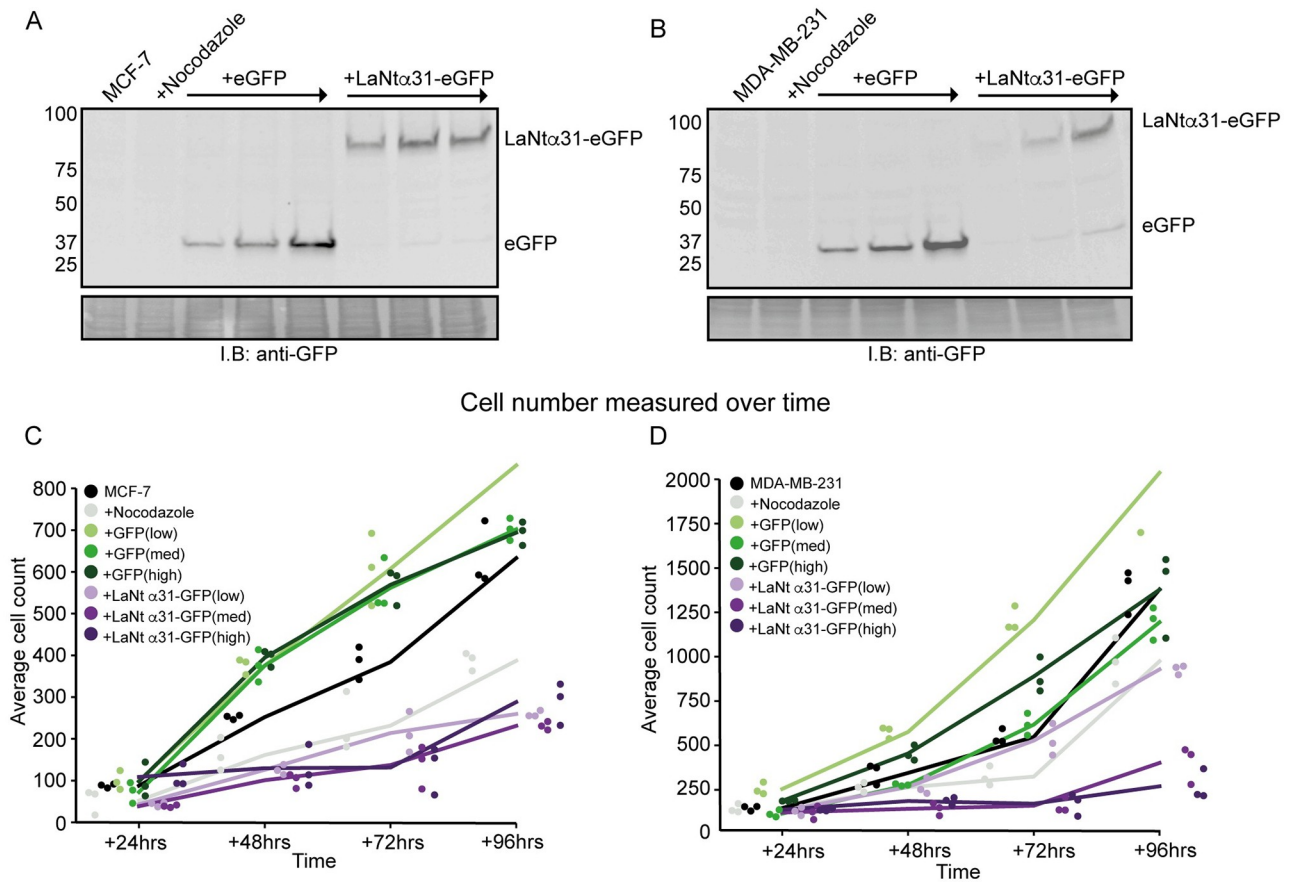


Fig 5. LaNt α 31 overexpression reduces proliferation rates. MCF-7 or MDA-MB-231 cells, either left untreated, treated with 20 ng mL⁻¹ nocodazole, or transduced with increasing doses of eGFP (+eGFP) or LAMA3LN1-eGFP (+LaNt α 31-eGFP) adenoviral particles, were cultured for 96 h following transduction and replating. (A) Immunoblots from total cell lysates for MCF-7 or MDA-MB-231 cells taken after 24 h were probed with antibodies against eGFP, with ponceau S total protein-stained membrane shown below. (B) Hoechst 33342 was added to the culture media, and the cell nuclei imaged after 20 min. Each dot represents an experimental repeat consisting of the mean of 3 fields of view per well for 3 technical replicates.

<https://doi.org/10.1371/journal.pone.0264430.g005>

qPCR normalised to GAPDH and RPLP0. Analysis revealed that cell proliferation is not required for LaNt α 31 transcript expression in either MCF7 (mean fold change relative to untreated cells \pm S.D: +2 h mitomycin c 1.2 ± 0.29 , +16 h mitomycin c 0.73 ± 0.12 $n \geq 4$. rANOVA on mean Δ Ct values, $p = 0.016$, not significant when adjusted for multiple comparisons, S2 Fig) or MDA-MB-231 cells (+2 h mitomycin c 1.1 ± 0.19 , MDA-MB-231 +16 h mitomycin c 0.89 ± 0.095 , $n \geq 4$. rANOVA on mean Δ Ct values, $p = 0.066$, S2 Fig).

Next, to determine whether LaNt α 31 upregulation influences cell proliferation, we used an adenoviral system to drive overexpression of LaNt α 31 tagged with eGFP (+LaNt α 31-eGFP) in MCF-7 and MDA-MB-231 (Fig 5A and 5B). Cells transduced with eGFP only were used to control for adenoviral transduction and eGFP expression. Viral load was functionally titred to achieve low, medium and high levels of expression (Fig 5A and 5B). Expression of LaNt α 31-eGFP caused a reduction in cell numbers in MCF-7 at all expression levels (Fig 5C and 5D, mean nuclei count at +96 h \pm S.D: untreated MCF-7 633 ± 80 , nocodazole 387 ± 70 , +eGFP low 855 ± 90 , +eGFP med 702 ± 60 , +eGFP high 694 ± 30 , +LaNt α 31-eGFP low 260 ± 10 , +LaNt α 31-eGFP med 231 ± 10 , +LaNt α 31-eGFP high 288 ± 50 . rANOVA controlling for multiple comparisons, $p = 0.004$). A similar reduction in cell numbers was also

identified in MDA-MB-231 cells (untreated MDA-MB-231 1379 ± 80 , +nocodazole 974 ± 20 , +eGFP low 2037 ± 90 , +eGFP med 1194 ± 30 , +eGFP high 1378 ± 30 , +LaNt α 31-eGFP low 928 ± 10 , +LaNt α 31-eGFP med 401 ± 10 , +LaNt α 31-eGFP high 270 ± 50 . rANOVA controlling for multiple comparisons, $p = 0.006$).

LaNt α 31 expression does not induce increased cell migration rates in low-migratory breast cancer cells

MCF-7 cells inherently migrate slowly [39–41]. This line was therefore used to assess if induction of LaNt α 31 expression increases migration. In gap closure assays (Fig 6A and 6B) and single cell migration assays (Fig 6C and 6D), no statistically significant differences were observed between MCF-7 cells expressing LaNt α 31 and controls (Gap closure: median MCF-7 83.3%, +eGFP 79.7%, +LaNt α 31-eGFP 80.2%, $p = 0.38$, Single cell assays: mean migration speed \pm S.D. MCF-7 $0.21 \mu\text{m min}^{-1} \pm 0.06$, +eGFP $0.21 \mu\text{m min}^{-1} \pm 0.05$, +LaNt α 31-eGFP $0.33 \mu\text{m min}^{-1} \pm 0.09$, $p = 0.53$, determined by rANOVA).

MCF7 cells also do not display inherent invasive behaviour [39–41]. We, therefore, next asked if increasing LaNt α 31 expression could induce invasive capabilities in MCF7 by using an inverted invasion assay [34, 42], where cells were seeded on the base of a porous membrane then stimulated to invade into a provided matrix and using an EGF gradient as a chemoattractant (Fig 6E–6H). As we hypothesised that LaNt α 31 effects could be LM specific, invasion into two different matrices were analysed; collagen I to mimic the interstitial matrix (Fig 6E and 6F) and Matrigel, a BM analogue that contains approximately 60% LM111, 30% Type IV collagen, and 8% entactin [35, 43] (Fig 6G and 6H). Untreated MCF-7 cells and cells transduced with either GFP or LaNt α 31-GFP each had very low invasive capabilities into either matrix type with no significant change in invasion depth between the different conditions (mean \pm S.D invasion depth into collagen I: MCF-7 $70 \mu\text{m} \pm 7$, +eGFP $67 \mu\text{m} \pm 4$, +LaNt α 31-eGFP $60 \mu\text{m} \pm 0$, $p = 0.22$, determined by ANOVA, Fig 6F. Into Matrigel: MCF-7 $55 \mu\text{m} \pm 0$, +eGFP $57 \mu\text{m} \pm 13$, +LaNt α 31-eGFP $58 \mu\text{m} \pm 6$, $p = 0.71$, determined by rANOVA, Fig 6H).

Increased LaNt α 31 expression causes a change in mode of invasion into laminin-rich hydrogels

In contrast to MCF7, MDA-MB-231 are much more motile and invasive [34, 42, 44]. The effects of induced LaNt α 31 expression on gap closure (Fig 7A and 7B) and single cell migration (Fig 7C and 7D) of MDA-MB-231 were below the threshold for statistical significance with one exception between eGFP and +LaNt α 31-GFP in single cell migration assays (Gap closure; median: MDA-MB-231 98.8%, +eGFP 92.7%, +LaNt α 31-eGFP 85.1%, $p = 0.23$, low density migration, mean speed \pm S.D: MDA-MB-231 $0.48 \mu\text{m min}^{-1} \pm 0.10$, +eGFP $0.50 \mu\text{m min}^{-1} \pm 0.2$, +LaNt α 31-eGFP $0.37 \mu\text{m min}^{-1} \pm 0.2$, MDA-MB-231 vs +LaNt α 31-eGFP, $p = 0.16$; +eGFP vs +LaNt α 31-eGFP, $p = 0.02$ determined by rANOVA with Bonferroni post hoc test.).

As expected, MDA-MB-231 invaded efficiently into collagen I and Matrigel matrices (Fig 8). The invasion depth of +LaNt α 31-eGFP MDA-MB-231 cells into collagen I was unchanged compared with controls (mean \pm S.D depth into collagen: MDA-MB-231 $89 \mu\text{m} \pm 21$, +eGFP $90 \mu\text{m} \pm 7$, +LaNt α 31-eGFP $83 \mu\text{m} \pm 18$, $p = 0.52$ rANOVA, Fig 8A and 8B). However, a small reduction was observed in the total invasion depth into Matrigel in the LaNt α 31 induced expression cells relative to controls (invasion into Matrigel: MDA-MB-231 $136 \mu\text{m} \pm 10$ S.D, +eGFP $127 \mu\text{m} \pm 4$, +LaNt α 31-eGFP $97 \mu\text{m} \pm 11$, MDA-MB-231 vs +LaNt α 31-eGFP $p = 0.005$, +eGFP vs +LaNt α 31-eGFP $p = 0.017$, rANOVA with Bonferroni post hoc test. Fig 8C and 8D).

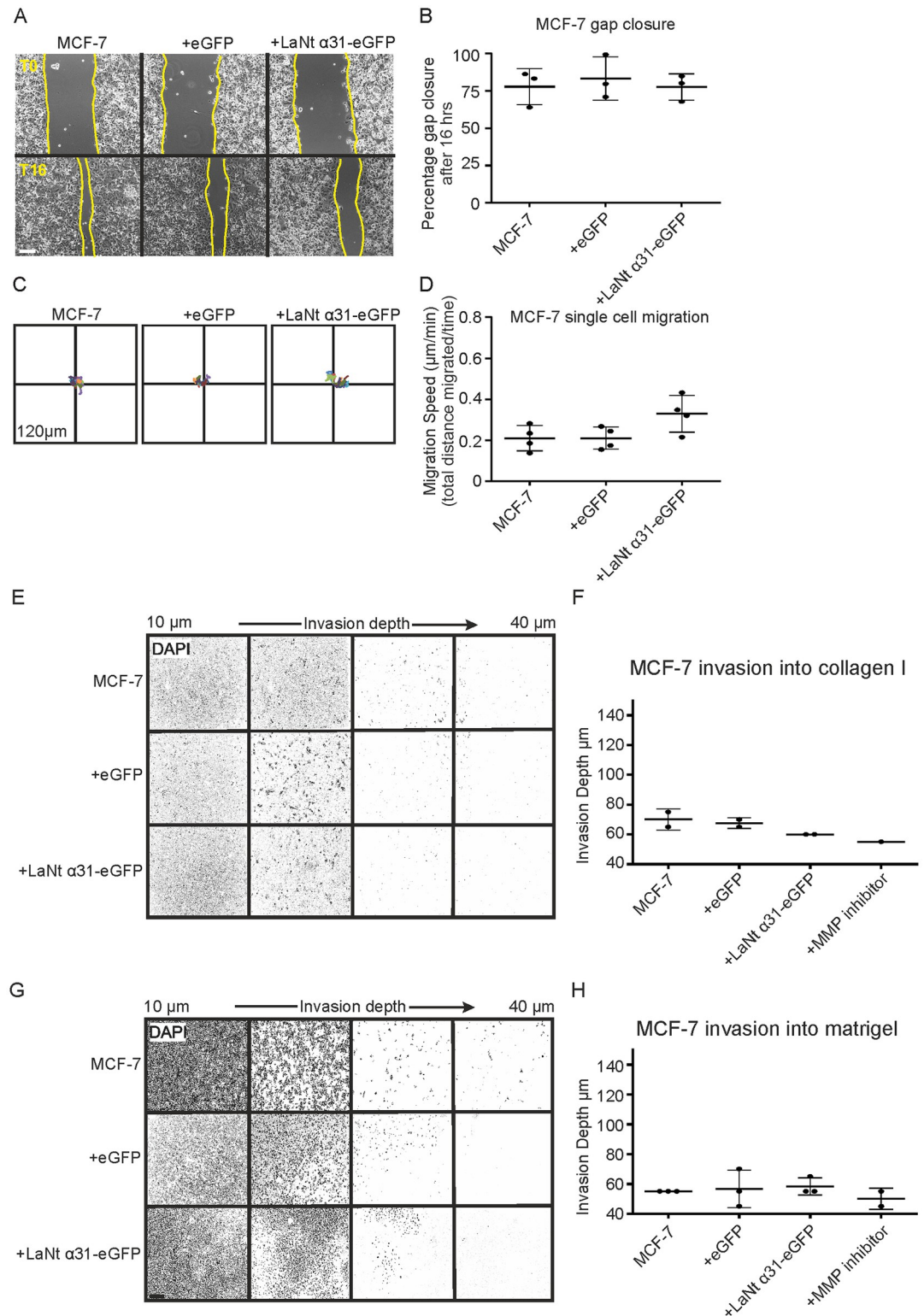


Fig 6. LaNt α 31 overexpression does not significantly affect 2D migration or 3D invasion of MCF-7 cells. MCF-7 cells were either left untreated or transduced with eGFP (+eGFP), or LAMA3LN1-eGFP (+LaNt α 31-eGFP). For gap closure assays, 24 h after transduction, cells were seeded into ibidi[®] 2-well culture inserts and allowed to attach for 6 h, the inserts were then removed, and the gap margin imaged at 0 h and 16 h. For single cell migration assays, 24 h after transduction, cells were seeded onto tissue culture plastic and the migration paths of individual cells tracked over a four-hour period. (A) Representative

images from immediately after removing chamber (T0 upper panels) and after 16 h (T16 lower panels), yellow lines delineate wound margins. (B) Gap closure was measured as a percentage relative to starting gap area. (C) Vector diagrams showing representative migration paths of 10 individual cells with each colour representing a single cell. (D) Migration speed was measured as total distance migrated over time. Each point on the associated dot plots represents an independent experiment with 2–3 technical replicates per experiment for gap closures assays or 20–40 cells per low density migration assay. For invasion assays, cells were plated onto the outside of a transwell membrane. 10 ng mL^{-1} epidermal growth factor was used to stimulate invasion through the membrane and into collagen I or Matrigel. After 48 h, the cells were fixed and stained with DAPI then imaged at $5 \mu\text{m}$ intervals using a spinning disk confocal microscope. (E and G) Representative images of invasion into collagen I or Matrigel from 10–40 μm presented at equal intervals. (F and H) Absolute invasion depth was measured where cell count ≥ 1 . Treatment with GM6001 MMP inhibitor was included as an invasion inhibiting control. Each point on the graphs represents an independent experiment, with 2–3 technical replicates per assay. Statistical tests of differences relative to controls were performed using one-way rANOVA followed by Bonferroni's post hoc analyses; $p > 0.05$ in all comparisons. Scale bar in (a) represents $100 \mu\text{m}$.

<https://doi.org/10.1371/journal.pone.0264430.g006>

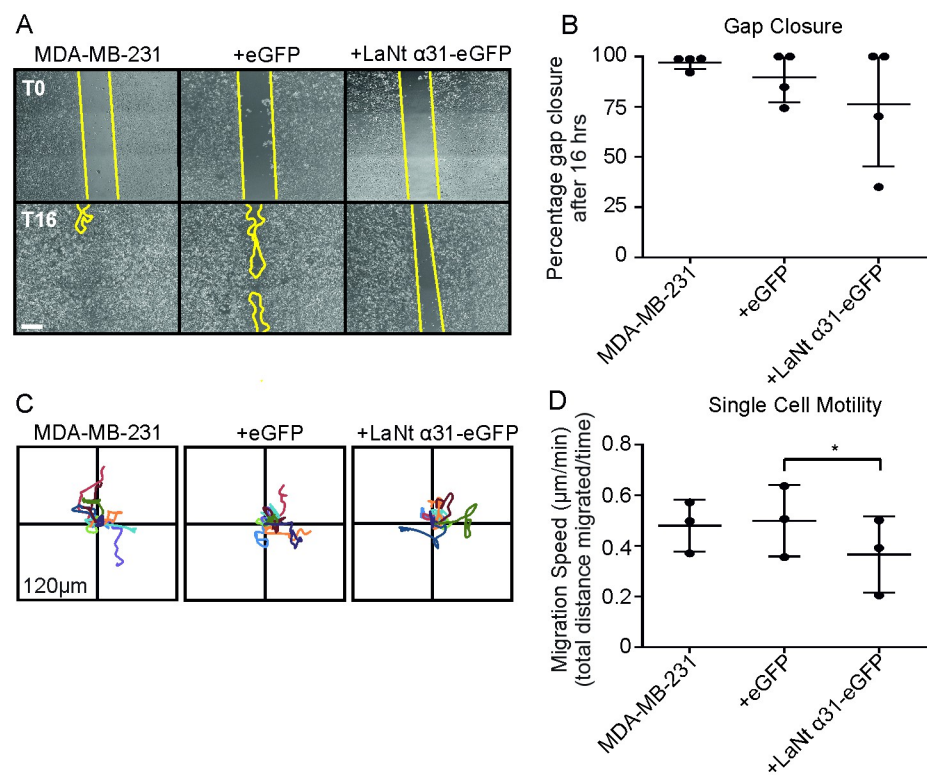


Fig 7. LaNt α 31 overexpression does not significantly affect 2D migration of MDA-MB-231 cells. MDA-MB-231 cells were either left untreated or transduced with eGFP (+eGFP), or LAMA3LN1-eGFP (+LaNt α 31-eGFP). For gap closure assays, 24 h after transduction, cells were seeded into ibidi[®] 2-well culture inserts and allowed to attach for 6 h, the inserts were then removed, and the gap margin imaged at 0 h and 16 h. For single cell migration assays, 24 h after transduction, cells were seeded onto tissue culture plastic and the migration paths of individual cells tracked over a four-hour period. (A) Representative images from immediately after removing chamber (T0 upper panels) and after 16 h (T16 lower panels), yellow lines delineate wound margins. (B) Gap closure was measured as a percentage relative to starting gap area. (C) Vector diagrams showing representative migration paths of 10 individual cells with each colour representing a single cell. (D) Migration speed was measured as total distance migrated over time. Each point on the associated dot plots represents an independent experiment with 2–3 technical replicates per experiment for gap closures assays or 20–40 cells per low density migration assay. Statistical tests of differences relative to controls were performed using one-way rANOVA followed by Bonferroni's post hoc tests; * $p < 0.05$. Scale bar in (a) represents $100 \mu\text{m}$.

<https://doi.org/10.1371/journal.pone.0264430.g007>

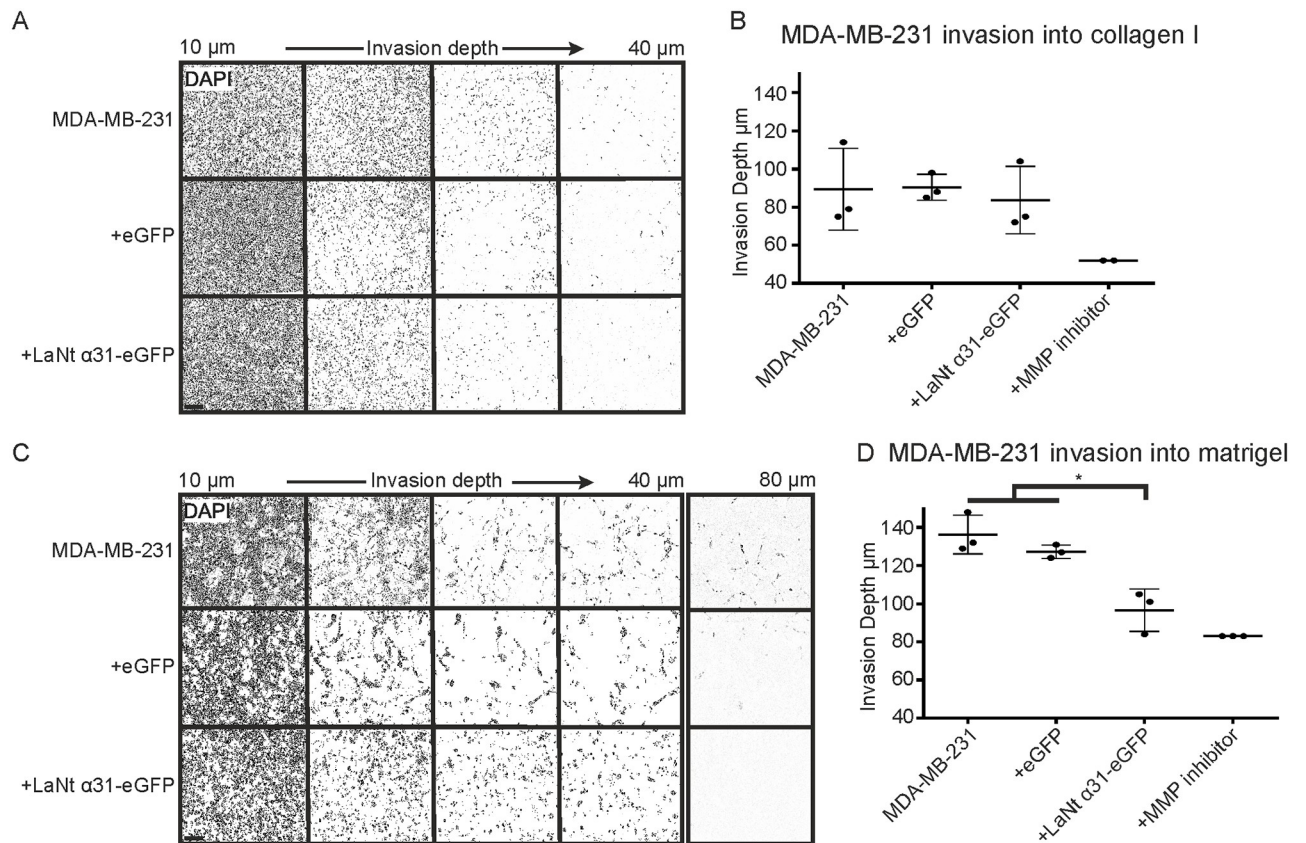


Fig 8. LaNt α 31 overexpression causes a small reduction in invasion of MDA-MB-231 cells into Matrigel. MDA-MB-231 cells, either left untreated or transduced with eGFP (+eGFP), or LAMA3LN1-eGFP (+LaNt α 31-eGFP), were plated onto the outside of a transwell membrane. 10 ng mL^{-1} epidermal growth factor was used to stimulate invasion through the membrane into collagen I (A-B) or Matrigel (C-D). After 48 h, the cells were fixed and DAPI stained then imaged at $5 \mu\text{m}$ intervals using a spinning disk confocal microscope. (A) and (C) Representative images from 10–40 μm depth presented at equal intervals, with an additional slice at 80 μm in (C). Absolute invasion depth was measured where cell count ≥ 1 . Treatment with GM6001 MMP inhibitor was included as an invasion inhibiting control. Each point on the graphs in (B) and (D) represents an independent experiment, with 2–3 technical replicates per assay. * represents $p < 0.05$ between bracketed groups as determined by one-way ANOVA followed by Bonferroni's post hoc analyses.

<https://doi.org/10.1371/journal.pone.0264430.g008>

Although the differences in invasion depth were relatively small, visual analysis of the Matrigel invasion assays revealed a clear and intriguing distinct phenotypic difference between the LaNt α 31 overexpressing cells compared with the controls (Figs 8C and 9A). Whereas MDA-MB-231 cells usually invade into Matrigel as multicellular streams, as has been reported previously [44, 45], the +LaNt α 31-eGFP cells did not display this behaviour (S1 and S2 Movies, maximum intensity projection Fig 9A). To assess this quantitatively, we wrote a macro to convert the DAPI stained images into a measure of cohesiveness at each depth (entropy) (Fig 9B). Between 50 and 65 μm depth, cell densities were similar between +LaNt α 31-eGFP and controls, therefore allowing direct comparison between lines. Across this depth range the level of cohesiveness was statistically significantly lower in the +LaNt α 31 MDA-MB-231 cells than in both control treatments (Mean+SD entropy MDA-MB-231 / +eGFP / +LaNt α 31-eGFP: 50 μm , 0.35 ± 0.09 , 0.37 ± 0.01 , 0.22 ± 0.04 ; 55 μm , 0.31 ± 0.09 , 0.32 ± 0.01 , 0.15 ± 0.04 ; 60 μm 0.27 ± 0.08 , 0.27 ± 0.01 , 0.11 ± 0.03 ; 65 μm 0.23 ± 0.08 , 0.22 ± 0.01 , 0.07 ± 0.02 , $p < 0.05$ compared for +LaNt α 31-eGFP compared with MDA-MB-231 and +eGFP for all depths between 50 and 65 μm , 2-way ANOVA Tukey's post hoc test, Fig 9C).

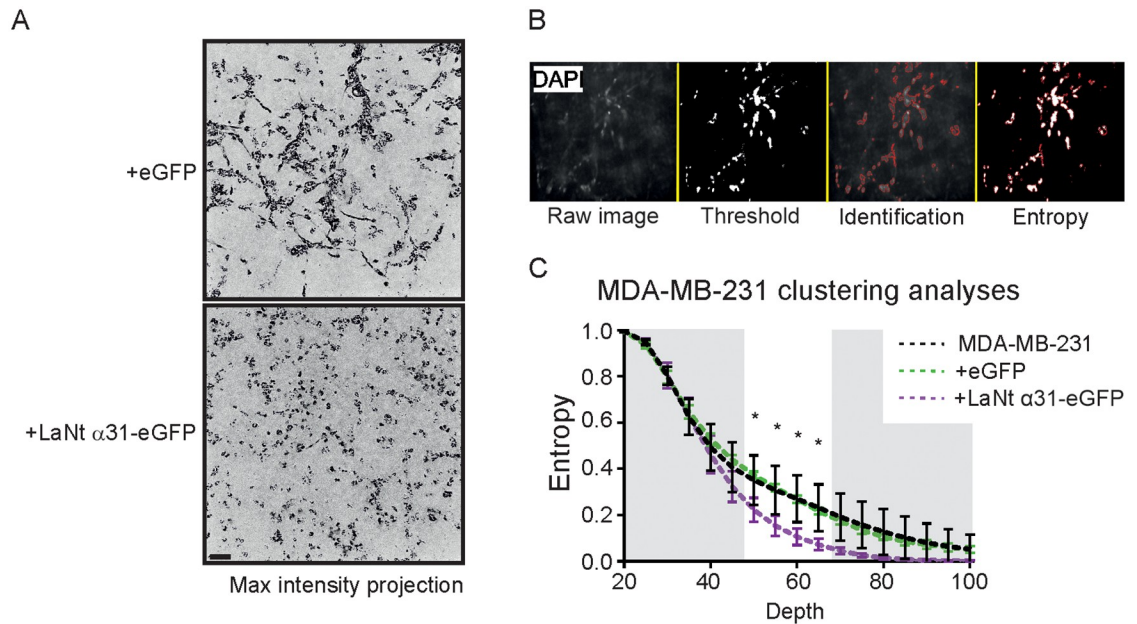


Fig 9. LaNt α 31 overexpression causes a change in mode of invasion of MDA-MB-231 cells into Matrigel. (A) Maximum intensity projection of planes from 20–60 μ m from the same assays in Fig 8C. (B) Image analyses method for determining entropy as a measure of cell clustering/cohesiveness; each stack of images was processed using an automated processing algorithm, where cell count and entropy score after a threshold was measured for each image in the stack. (C) Entropy score versus depth graph with points representing mean and SD from 3 independent experiments. Shaded regions indicate where comparisons lack value due to either high cell counts (0–45 μ m) or differences in cell numbers between conditions (>70 μ m). * denote statistically significant differences between +LaNt α 31-GFP cells and both MDA-MB-231 and +GFP conditions by 2-way ANOVA with Tukey's post hoc test.

<https://doi.org/10.1371/journal.pone.0264430.g009>

Tumours with high LaNt α 31 expression are likely to be non-cohesive

As the LaNt α 31 functional studies data suggested that high expression of this protein changes the mode of tumour invasion, we returned to the tissue array data, focusing specifically on the cores with high LaNt α 31 intensity and assessed the tumour appearance in each of those cores as either “cohesive” or “non-cohesive” depending on whether tumour cells were present in contiguous islands with well-defined borders, (representative examples Fig 10A). These analyses revealed that 67.7% of the high LaNt α 31 expressing tumours were non-cohesive in appearance (21 of 31 cores, Fig 10B).

Discussion

The findings presented here have revealed that the little-known LM-related protein LaNt α 31 is upregulated in a distinct sub-population of breast cancers, including a subset of TNBC, and correlates with tumour cohesiveness but is not predictive of nodal involvement. In vitro studies revealed that LaNt α 31 expression was not sufficient to confer invasive nor increased migratory capabilities into a non-invasive breast cancer cell line; however, LaNt α 31 expression converted the mode of invasion of an already invasive line when invading into a LM-rich matrix. These findings are consistent with a potential effect of LaNt α 31 upon tumour cohesiveness and suggest that dysregulation of this protein could actively contribute to defining how breast cancer cells disseminate.

Usually in tumour situations, very few cells acquire the ability to invade and a hallmark of more aggressive tumours is plasticity in the modes of migration [46, 47]. A switch from

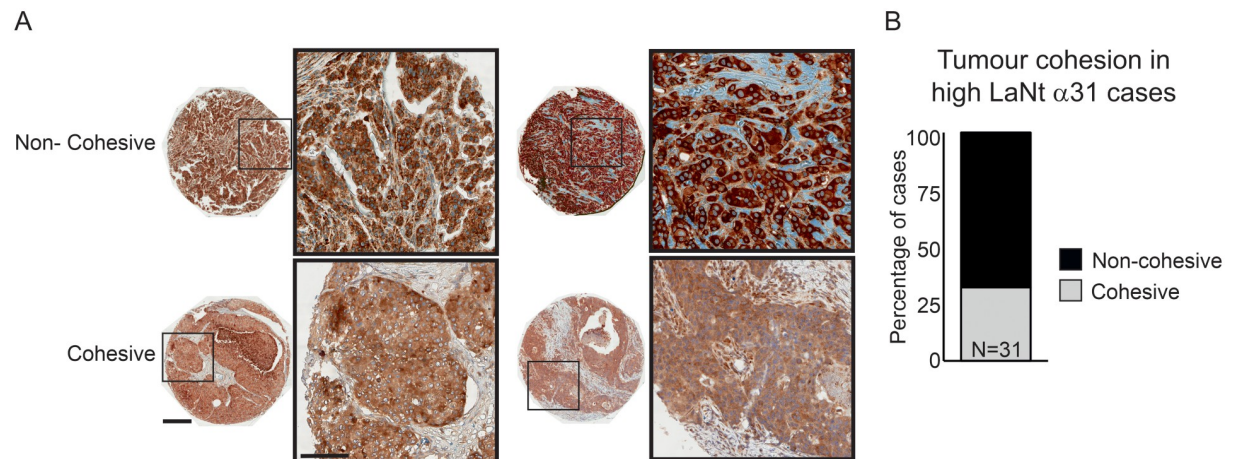


Fig 10. High LaNt α 31 expression is associated with low tumour cohesion in invasive ductal carcinoma. Formalin-fixed paraffin embedded human breast tissue microarray sections processed for immunohistochemistry with mouse monoclonal antibodies against LaNt α 31. Tumour cohesion was graded as either cohesive (tight tumour islands), or non-cohesive (chord-like) in tumour cores scored as having high LaNt α 31 expression. (A) Representative example of core grading. (B) Stacked column graphs of percentage of cases that are either cohesive or non-cohesive. Scale bars: 300 μ m.

<https://doi.org/10.1371/journal.pone.0264430.g010>

multicellular streaming to individual cell invasion can happen in multiple overlapping ways. A major driver is the mechanical properties of the ECM including matrix stiffness and the orientation of fibres; however decreased cell-cell adhesion, increased Rac-driven cytoskeletal protrusion compared with Rho-mediated contraction, an increased ability to generate traction forces, and differences in proteolytic activities all can drive the changes [44], as reviewed in [48]. Many of these mechanisms are intrinsically linked, which makes it challenging to directly assign a single behaviour to an individual protein. However, the Matrigel-specific effects and the structural similarity between netrin-4 and LaNt α 31 make it tempting to predict that LaNt α 31 has a disruptive effect on LM networks, softening or disordering the matrix through which the cells are invading and providing a permissive environment for tumour metastasis [19, 21].

The differences in responses between MCF7 and MDA-MB-231 could also provide support for a matrix-disruptive mechanism. MDA-MB-231 are more mesenchymal-like compared with the more epithelial-like MCF7, and this is associated with their intrinsic differences in migration behaviours; individual cell migration and multicellular streaming for MDA-MB-231, versus collective for MCF7. The invasive MDA-MB-231 line when cultured on Matrigel has also been reported to express much higher levels of MMP9 than MCF7s, and this expression is required for their invasive capabilities [49]. LN domains, including the LN domain of LM α 3b, are known to have cell-surface receptor-binding capabilities [50] [51]. Notably, netrin-4 and a proteolytically released LN domain fragment of LM β 1 are each capable of inducing epithelial to mesenchymal transition and have been shown to regulate expression of MMPs [19, 20, 52, 53]. Therefore, the LaNt α 31 effect could be an indirect consequence of cell receptor activation through a similar but as yet unidentified mechanism. Matrigel also contains many components beyond LM111 [43], therefore the observed invasion phenotype could be due to LaNt α 31 interaction with additional non-LM factors. Dissecting the mechanism of the LaNt α 31-induced changes will not be a trivial undertaking but will be valuable to understand the processes involved. Moreover, *in vivo* analyses will be required to determine the contribution to tumour progression of LaNt α 31 and to identify any cause-and-effect relationship

between LaNt α 31 expression and tumour cohesiveness, and the importance of these effects to tumour progression.

One finding that has been hard to reconcile is despite the association between high LaNt α 31 expression and cancer and increased LaNt α 31 expression in metastasis relative to primary tumours, there were no statistically robust associations between LaNt α 31 expression level and nodal involvement or patient survival. This collection of findings is somewhat counter-intuitive and while they may be indicative of a true lack of effect of LaNt α 31 on patient outcome, the data may also point to more complex subtype effects that are not captured by our limited molecular phenotyping data and by sample sizes which were not amenable to further subgroup analyses. Subsequent analyses may be warranted with stratification on markers such as EGFR, as this could provide indications of mechanism. It may also now be valuable to now assess co-distribution patterns of putative LaNt, netrin and laminin receptors.

Secondly, while the tissue data immunohistochemistry results indicated that tumours with high Ki67 percentage were more likely to display medium to high LaNt α 31 immunoreactivity, stratification by proliferation status of the underlying tumour did not improve predictions of nodal involvement. Moreover, the *in vitro* studies indicated that LaNt α 31 expression is not dependent on proliferation, and that induced expression reduced rather than increased cell numbers both in MCF7 and in MDA-MB-231 cells in culture. Together these findings could suggest that the Ki67/ LaNt α 31 expression could be a spurious correlation. However, it should be noted that the *in vitro* work only involved epithelial-derived tumour cells cultured on solid 2-D substrates and does not account for the complex tumour environment. The ostensibly disparate findings in tumour sections compared with cultured cells may reflect the LaNt α 31 protein acting on the matrix, influencing matrix stiffness, pore size or signal propagation, and thereby LaNt α 31 may indirectly influence cell cycle progression when in its true biological context. This is a complex question, requiring advanced *in vivo* models to address, and will be the focus of future work.

An additional intriguing finding was the difference between LaNt α 31 and LM α 3. Although these proteins are genetically linked, they are structurally and functionally distinct. Specifically, LM α 3a, as part of LM332, has been robustly demonstrated to enhance the migratory behaviour of MCF7 and MDA-MB-231 cells in culture [54, 55]. However, loss or focal disruption of LM332 staining is a more common feature in breast cancer, particularly for LM α 3b, which shares a promoter with LaNt α 31, and is downregulated in the tumour vasculature [26]. Indeed, in side-by-side comparison of the same tissue, the observation of different structures displaying upregulation of LaNt α 31 compared with LM α 3 points to differences in post-transcriptional regulation. We do not yet know if the difference is due to differences between the isoforms in terms of pre-mRNA processing, mRNA degradation, or post-translational proteolytic processing; however, these data do suggest that changes to LaNt α 31 expression may have more widespread implications to other cancer subtypes where LM α 3 is known to be dysregulated. In these contexts, processing tissue for LaNt α 31 may have value as a biomarker.

Conclusions

The combination of patient and experimental data presented here have revealed for the first time that LaNt α 31 is associated with breast cancer. Importantly, that LaNt α 31 influences the mechanisms through which invasive breast cancer cells migrate in a 3-D environment. These findings suggest that LaNt α 31 contributes to how a tumour progresses and raises the potential that targeting this protein's function could hold therapeutic value.

Supporting information

S1 Fig. LaNt α 31 is upregulated in ductal carcinoma and in lymph node metastases. Formalin-fixed paraffin-embedded human breast tissue microarray sections processed for immunohistochemistry with mouse monoclonal antibodies against LaNt α 31. Two separate arrays were used; (A) uninvolved with paired invasive/ in situ ductal carcinoma tissues (N = 25), (B) invasive ductal carcinoma with paired node metastases (N = 29). All paired cores analysed in Fig 2 ordered based on LaNt α 31 staining intensity, low to high (left to right). Scale bars: 500 μ m.

(TIF)

S2 Fig. Proliferation is not required for LaNt α 31 expression. MCF-7 or MDA-MB-231 cells were treated with 10 μ g mL⁻¹ mitomycin c for either 2 h or left with the drug overnight. (A) Hoechst 33342 was added to the culture media, and the cell nuclei imaged after 20 min. (B) After 24 h, total RNA was extracted and one-step RT-qPCR performed to quantify LAMA3LN1 transcript abundance, normalising to GAPDH and RPLP0 reference transcripts.

(TIF)

S3 Fig. Uncropped immunoblot and qRT-PCR melt curves.

(TIF)

S1 Movie. MDA-MB-231 +eGFP invasion into Matrigel. MDA-MB-231 cells transduced with eGFP were plated onto the outside of a transwell membrane. 10 ng mL⁻¹ epidermal growth factor was used to stimulate invasion through the membrane and into Matrigel. After 48 h, the cells were fixed and stained with DAPI then imaged at 5 μ m intervals using a spinning disk confocal microscope. Representative movie of invasion profile generated from z-stack slices for invasion between 20 and 60 μ m after applying threshold.

(AVI)

S2 Movie. MDA-MB-231 +LaNt α 31-eGFP invasion into Matrigel. MDA-MB-231 cells transduced with LaNt α 31-eGFP were plated onto the outside of a transwell membrane. 10 ng mL⁻¹ epidermal growth factor was used to stimulate invasion through the membrane and into Matrigel. After 48 h, the cells were fixed and stained with DAPI then imaged at 5 μ m intervals using a spinning disk confocal microscope. Representative movie of invasion profile generated from z-stack slices for invasion between 20 and 60 μ m after applying threshold.

(AVI)

S1 Raw images.

(TIF)

Acknowledgments

The authors would also like to thank Bryan Williams for his help in writing image analysis macro, Abigail Pickett, Marian Jones, Eleanor Hughes, and Louisa Orfanou for their help in image scoring, and Louise Brown for help with the invasion assays. The authors would like to acknowledge the donors, without whom this work would not be possible.

Author Contributions

Conceptualization: Lee D. Troughton, Kevin J. Hamill.

Data curation: Lee D. Troughton, Danielle A. O'Loughlin.

Formal analysis: Lee D. Troughton, Danielle A. O'Loughlin, Kevin J. Hamill.

Funding acquisition: Kevin J. Hamill.

Investigation: Lee D. Troughton, Tobias Zech.

Methodology: Lee D. Troughton, Tobias Zech.

Project administration: Lee D. Troughton, Kevin J. Hamill.

Resources: Kevin J. Hamill.

Writing – original draft: Lee D. Troughton, Tobias Zech, Kevin J. Hamill.

Writing – review & editing: Lee D. Troughton, Danielle A. O’Loughlin, Tobias Zech, Kevin J. Hamill.

References

1. Hanahan D, Weinberg RA. The hallmarks of cancer. *Cell*. 2000; 100(1):57–70. Epub 2000/01/27. [https://doi.org/10.1016/s0092-8674\(00\)81683-9](https://doi.org/10.1016/s0092-8674(00)81683-9) PMID: 10647931.
2. Sidhom G, Imam M. Evaluation of serum laminin as a tumor marker in breast cancer. *Int J Clin Lab Res*. 1999; 29(1):26–9. Epub 1999/06/05. <https://doi.org/10.1007/s005990050058> PMID: 10356660.
3. Giussani M, Landoni E, Merlino G, Turdo F, Veneroni S, Paolini B, et al. Extracellular matrix proteins as diagnostic markers of breast carcinoma. *J Cell Physiol*. 2018; 233(8):6280–90. Epub 2018/03/10. <https://doi.org/10.1002/jcp.26513> PMID: 29521413.
4. Moriggi M, Giussani M, Torretta E, Capitanio D, Sandri M, Leone R, et al. ECM Remodeling in Breast Cancer with Different Grade: Contribution of 2D-DIGE Proteomics. *Proteomics*. 2018; 18(24): e1800278. Epub 2018/10/26. <https://doi.org/10.1002/pmic.201800278> PMID: 30353998.
5. Holler E. Laminin isoform expression in breast tumors. *Breast Cancer Res*. 2005; 7(4):166–7. Epub 2005/07/01. <https://doi.org/10.1186/bcr1270> PMID: 15987470.
6. Brassart-Pasco S, Brezillon S, Brassart B, Ramont L, Oudart JB, Monboisse JC. Tumor Microenvironment: Extracellular Matrix Alterations Influence Tumor Progression. *Front Oncol*. 2020; 10:397. Epub 2020/05/01. <https://doi.org/10.3389/fonc.2020.00397> PMID: 32351878.
7. Hohenester E, Yurchenco PD. Laminins in basement membrane assembly. *Cell adhesion & migration*. 2013; 7(1):56–63. Epub 2012/10/19. <https://doi.org/10.4161/cam.21831> PMID: 23076216.
8. Hamill KJ, Kligys K, Hopkinson SB, Jones JC. Laminin deposition in the extracellular matrix: a complex picture emerges. *Journal of cell science*. 2009; 122(Pt 24):4409–17. Epub 2009/12/04. <https://doi.org/10.1242/jcs.041095> PMID: 19955338.
9. Patarroyo M, Tryggvason K, Virtanen I. Laminin isoforms in tumor invasion, angiogenesis and metastasis. *Semin Cancer Biol*. 2002; 12(3):197–207. Epub 2002/06/27. [https://doi.org/10.1016/S1044-579X\(02\)00023-8](https://doi.org/10.1016/S1044-579X(02)00023-8) PMID: 12083850.
10. Rousselle P, Scoazec JY. Laminin 332 in cancer: When the extracellular matrix turns signals from cell anchorage to cell movement. *Semin Cancer Biol*. 2019. Epub 2019/10/23. <https://doi.org/10.1016/j.semcancer.2019.09.026> PMID: 31639412.
11. Hamill KJ, Langbein L, Jones JC, McLean WH. Identification of a novel family of laminin N-terminal alternate splice isoforms: structural and functional characterization. *J Biol Chem*. 2009; 284(51):35588–96. Epub 2009/09/24. <https://doi.org/10.1074/jbc.M109.052811> PMID: 19773554.
12. Barrera V, Troughton LD, Iorio V, Liu S, Oyewole O, Sheridan CM, et al. Differential Distribution of Laminin N-Terminus α 31 Across the Ocular Surface: Implications for Corneal Wound Repair. *Invest Ophthalmol Vis Sci*. 2018; 59(10):4082–93. Epub 2018/08/12. <https://doi.org/10.1167/iovs.18-24037> PMID: 30098195.
13. Aumailley M, Bruckner-Tuderman L, Carter WG, Deutzmann R, Edgar D, Ekblom P, et al. A simplified laminin nomenclature. *Matrix Biol*. 2005; 24(5):326–32. Epub 2005/06/28. <https://doi.org/10.1016/j.matbio.2005.05.006> PMID: 15979864.
14. Ryan MC, Tizard R, VanDevanter DR, Carter WG. Cloning of the LamA3 gene encoding the α 3 chain of the adhesive ligand epiligrin. Expression in wound repair. *J Biol Chem*. 1994; 269(36):22779–87. Epub 1994/09/09. PMID: 8077230.
15. Miner JH, Patton BL, Lentz SI, Gilbert DJ, Snider WD, Jenkins NA, et al. The laminin α chains: expression, developmental transitions, and chromosomal locations of α 1–5, identification of heterotrimeric laminins 8–11, and cloning of a novel α 3 isoform. *J Cell Biol*. 1997; 137(3):685–701. Epub 1997/05/05. <https://doi.org/10.1083/jcb.137.3.685> PMID: 9151674.

16. Iorio V, Troughton LD, Barrera V, Hamill K. LaNt α 31 modulates LM332 organisation during matrix deposition leading to cell-matrix adhesion and migration defects. *bioRxiv*. 2019. <https://doi.org/10.1101/617597>
17. Cheng YS, Champlaud MF, Burgeson RE, Marinkovich MP, Yurchenco PD. Self-assembly of laminin isoforms. *J Biol Chem*. 1997; 272(50):31525–32. Epub 1998/02/12. <https://doi.org/10.1074/jbc.272.50.31525> PMID: 9395489
18. Yurchenco PD, Cheng YS. Laminin self-assembly: a three-arm interaction hypothesis for the formation of a network in basement membranes. *Contrib Nephrol*. 1994; 107:47–56. Epub 1994/01/01. <https://doi.org/10.1159/000422960> PMID: 8004974.
19. Schneiders FI, Maertens B, Bose K, Li Y, Brunken WJ, Paulsson M, et al. Binding of netrin-4 to laminin short arms regulates basement membrane assembly. *J Biol Chem*. 2007; 282(33):23750–8. Epub 2007/06/26. <https://doi.org/10.1074/jbc.M703137200> PMID: 17588941.
20. Staquicini FI, Dias-Neto E, Li J, Snyder EY, Sidman RL, Pasqualini R, et al. Discovery of a functional protein complex of netrin-4, laminin gamma1 chain, and integrin alpha6beta1 in mouse neural stem cells. *Proc Natl Acad Sci U S A*. 2009; 106(8):2903–8. Epub 2009/02/06. <https://doi.org/10.1073/pnas.0813286106> PMID: 19193855.
21. Reuten R, Patel TR, McDougall M, Rama N, Nikodemus D, Gibert B, et al. Structural decoding of netrin-4 reveals a regulatory function towards mature basement membranes. *Nature communications*. 2016; 7:13515. Epub 2016/12/03. <https://doi.org/10.1038/ncomms13515> PMID: 27901020.
22. Reuten R, Zendeheroud S, Nicolau M, Fleischhauer L, Laitala A, Kiderlen S, et al. Basement membrane stiffness determines metastases formation. *Nat Mater*. 2021. Epub 2021/01/27. <https://doi.org/10.1038/s41563-020-00894-0> PMID: 33495631.
23. Bergstraesser LM, Srinivasan G, Jones JC, Stahl S, Weitzman SA. Expression of hemidesmosomes and component proteins is lost by invasive breast cancer cells. *Am J Pathol*. 1995; 147(6):1823–39. Epub 1995/12/01. PMID: 7495306.
24. Martin KJ, Kwan CP, Nagasaki K, Zhang X, O'Hare MJ, Kaelin CM, et al. Down-regulation of laminin-5 in breast carcinoma cells. *Mol Med*. 1998; 4(9):602–13. Epub 1998/12/16. PMID: 9848077.
25. Henning K, Berndt A, Katenkamp D, Kosmehl H. Loss of laminin-5 in the epithelium-stroma interface: an immunohistochemical marker of malignancy in epithelial lesions of the breast. *Histopathology*. 1999; 34(4):305–9. Epub 1999/05/07. <https://doi.org/10.1046/j.1365-2559.1999.00634.x> PMID: 10231397.
26. Mori T, Kariya Y, Komiya E, Higashi S, Miyagi Y, Sekiguchi K, et al. Downregulation of a newly identified laminin, laminin-3B11, in vascular basement membranes of invasive human breast cancers. *Cancer Sci*. 2011; 102(5):1095–100. Epub 2011/02/01. <https://doi.org/10.1111/j.1349-7006.2011.01892.x> PMID: 21276136.
27. Carpenter PM, Wang-Rodriguez J, Chan OT, Wilczynski SP. Laminin 5 expression in metaplastic breast carcinomas. *Am J Surg Pathol*. 2008; 32(3):345–53. Epub 2008/02/28. <https://doi.org/10.1097/PAS.0b013e3181592201> PMID: 18300817.
28. Troughton LD, Reuten R, Sugden CJ, Hamill KJ. Laminin N-terminus alpha31 protein distribution in adult human tissues. *PLoS One*. 2020; 15(12):e0239889. Epub 2020/12/03. <https://doi.org/10.1371/journal.pone.0239889> PMID: 33264294.
29. Soule HD, Vazquez J, Long A, Albert S, Brennan M. A human cell line from a pleural effusion derived from a breast carcinoma. *J Natl Cancer Inst*. 1973; 51(5):1409–16. Epub 1973/11/01. <https://doi.org/10.1093/jnci/51.5.1409> PMID: 4357757.
30. Cailleau R, Young R, Olive M, Reeves WJ Jr. Breast tumor cell lines from pleural effusions. *J Natl Cancer Inst*. 1974; 53(3):661–74. Epub 1974/09/01. <https://doi.org/10.1093/jnci/53.3.661> PMID: 4412247.
31. Livak KJ, Schmittgen TD. Analysis of relative gene expression data using real-time quantitative PCR and the 2⁻(Delta Delta C(T)) Method. *Methods*. 2001; 25(4):402–8. Epub 2002/02/16. <https://doi.org/10.1006/meth.2001.1262> PMID: 11846609.
32. Oppelt A, Haugsten EM, Zech T, Danielsen HE, Sveen A, Lobert VH, et al. PIKfyve, MTMR3 and their product PtdIns5P regulate cancer cell migration and invasion through activation of Rac1. *Biochem J*. 2014; 461(3):383–90. Epub 2014/05/21. <https://doi.org/10.1042/BJ20140132> PMID: 24840251.
33. Garcia E, Ragazzini C, Yu X, Cuesta-Garcia E, Bernardino de la Serna J, Zech T, et al. WIP and WICH/WIRE co-ordinately control invadopodium formation and maturation in human breast cancer cell invasion. *Sci Rep*. 2016; 6:23590. Epub 2016/03/25. <https://doi.org/10.1038/srep23590> PMID: 27009365.
34. MacDonald E, Brown L, Selvais A, Liu H, Waring T, Newman D, et al. HRS-WASH axis governs actin-mediated endosomal recycling and cell invasion. *J Cell Biol*. 2018; 217(7):2549–64. Epub 2018/06/13. <https://doi.org/10.1083/jcb.201710051> PMID: 29891722.
35. Kleinman HK, Martin GR. Matrigel: basement membrane matrix with biological activity. *Semin Cancer Biol*. 2005; 15(5):378–86. Epub 2005/06/25. <https://doi.org/10.1016/j.semcancer.2005.05.004> PMID: 15975825.

36. Lu Z, Jiang G, Blume-Jensen P, Hunter T. Epidermal growth factor-induced tumor cell invasion and metastasis initiated by dephosphorylation and downregulation of focal adhesion kinase. *Mol Cell Biol*. 2001; 21(12):4016–31. Epub 2001/05/22. <https://doi.org/10.1128/MCB.21.12.4016-4031.2001> PMID: 11359909.
37. Gerdes J, Lemke H, Baisch H, Wacker HH, Schwab U, Stein H. Cell cycle analysis of a cell proliferation-associated human nuclear antigen defined by the monoclonal antibody Ki-67. *J Immunol*. 1984; 133(4):1710–5. Epub 1984/10/01. PMID: 6206131.
38. Dowsett M, Nielsen TO, A'Hern R, Bartlett J, Coombes RC, Cuzick J, et al. Assessment of Ki67 in breast cancer: recommendations from the International Ki67 in Breast Cancer working group. *J Natl Cancer Inst*. 2011; 103(22):1656–64. Epub 2011/10/01. <https://doi.org/10.1093/jnci/djr393> PMID: 21960707.
39. Kligys K, Wu Y, Hamill KJ, Lewandowski KT, Hopkinson SB, Budinger GR, et al. Laminin-332 and alpha3beta1 integrin-supported migration of bronchial epithelial cells is modulated by fibronectin. *Am J Respir Cell Mol Biol*. 2013; 49(5):731–40. Epub 2013/04/18. <https://doi.org/10.1165/rcmb.2012-0509OC> PMID: 23590307.
40. Hamill KJ, Hopkinson SB, Hoover P, Todorovic V, Green KJ, Jones JC. Fibronectin expression determines skin cell motile behavior. *J Invest Dermatol*. 2012; 132(2):448–57. Epub 2011/10/01. <https://doi.org/10.1038/jid.2011.297> PMID: 21956124.
41. Hamill KJ, Hiroyasu S, Colburn ZT, Ventrella RV, Hopkinson SB, Skalli O, et al. Alpha actinin-1 regulates cell-matrix adhesion organization in keratinocytes: consequences for skin cell motility. *J Invest Dermatol*. 2015; 135(4):1043–52. Epub 2014/11/29. <https://doi.org/10.1038/jid.2014.505> PMID: 25431851.
42. Yu X, Zech T, McDonald L, Gonzalez EG, Li A, Macpherson I, et al. N-WASP coordinates the delivery and F-actin-mediated capture of MT1-MMP at invasive pseudopods. *J Cell Biol*. 2012; 199(3):527–44. Epub 2012/10/24. <https://doi.org/10.1083/jcb.201203025> PMID: 23091069.
43. Hughes CS, Postovit LM, Lajoie GA. Matrigel: a complex protein mixture required for optimal growth of cell culture. *Proteomics*. 2010; 10(9):1886–90. Epub 2010/02/18. <https://doi.org/10.1002/pmic.200900758> PMID: 20162561.
44. Wolf K, Wu YI, Liu Y, Geiger J, Tam E, Overall C, et al. Multi-step pericellular proteolysis controls the transition from individual to collective cancer cell invasion. *Nat Cell Biol*. 2007; 9(8):893–904. Epub 2007/07/10. <https://doi.org/10.1038/ncb1616> PMID: 17618273.
45. Scott RW, Hooper S, Crighton D, Li A, Konig I, Munro J, et al. LIM kinases are required for invasive path generation by tumor and tumor-associated stromal cells. *J Cell Biol*. 2010; 191(1):169–85. Epub 2010/09/30. <https://doi.org/10.1083/jcb.201002041> PMID: 20876278.
46. Pinner S, Sahai E. Imaging amoeboid cancer cell motility in vivo. *J Microsc*. 2008; 231(3):441–5. Epub 2008/08/30. <https://doi.org/10.1111/j.1365-2818.2008.02056.x> PMID: 18754999.
47. Farina KL, Wyckoff JB, Rivera J, Lee H, Segall JE, Condeelis JS, et al. Cell motility of tumor cells visualized in living intact primary tumors using green fluorescent protein. *Cancer Res*. 1998; 58(12):2528–32. Epub 1998/07/04. PMID: 9635573.
48. Friedl P, Wolf K. Plasticity of cell migration: a multiscale tuning model. *J Cell Biol*. 2010; 188(1):11–9. Epub 2009/12/03. <https://doi.org/10.1083/jcb.200909003> PMID: 19951899.
49. Balduyck M, Zerimech F, Gouyer V, Lemaire R, Hemon B, Grard G, et al. Specific expression of matrix metalloproteinases 1, 3, 9 and 13 associated with invasiveness of breast cancer cells in vitro. *Clin Exp Metastasis*. 2000; 18(2):171–8. Epub 2001/03/10. <https://doi.org/10.1023/a:1006762425323> PMID: 11235993.
50. Garbe JH, Gohring W, Mann K, Timpl R, Sasaki T. Complete sequence, recombinant analysis and binding to laminins and sulphated ligands of the N-terminal domains of laminin alpha3B and alpha5 chains. *Biochem J*. 2002; 362(Pt 1):213–21. Epub 2002/02/07. <https://doi.org/10.1042/0264-6021:3620213> PMID: 11829758.
51. Kariya Y, Yasuda C, Nakashima Y, Ishida K, Tsubota Y, Miyazaki K. Characterization of laminin 5B and NH2-terminal proteolytic fragment of its alpha3B chain: promotion of cellular adhesion, migration, and proliferation. *J Biol Chem*. 2004; 279(23):24774–84. Epub 2004/03/27. <https://doi.org/10.1074/jbc.M400670200> PMID: 15044476.
52. Horejs CM, Serio A, Purvis A, Gormley AJ, Bertazzo S, Poliniewicz A, et al. Biologically-active laminin-111 fragment that modulates the epithelial-to-mesenchymal transition in embryonic stem cells. *Proc Natl Acad Sci U S A*. 2014; 111(16):5908–13. Epub 2014/04/08. <https://doi.org/10.1073/pnas.1403139111> PMID: 24706882.
53. Xu X, Yan Q, Wang Y, Dong X. NTN4 is associated with breast cancer metastasis via regulation of EMT-related biomarkers. *Oncol Rep*. 2017; 37(1):449–57. Epub 2016/11/15. <https://doi.org/10.3892/or.2016.5239> PMID: 27840993.

54. Plopper GE, Domanico SZ, Cirulli V, Kiosses WB, Quaranta V. Migration of breast epithelial cells on Laminin-5: differential role of integrins in normal and transformed cell types. *Breast Cancer Res Treat.* 1998; 51(1):57–69. Epub 1999/01/07. <https://doi.org/10.1023/a:1006086218174> PMID: 9877029.
55. Carpenter PM, Sivadas P, Hua SS, Xiao C, Gutierrez AB, Ngo T, et al. Migration of breast cancer cell lines in response to pulmonary laminin 332. *Cancer Med.* 2017; 6(1):220–34. Epub 2016/11/24. <https://doi.org/10.1002/cam4.957> PMID: 27878981.